Carbon Trends 11 (2023) 100265

Contents lists available at ScienceDirect

Carbon Trends

journal homepage: www.elsevier.com/locate/cartre

Parametric analysis of the coating thickness development of electrophoretically deposited carbon nanotube coatings

Timothy MacLucas[a,*], Silas Schütz[a], Sebastian Suarez[a], Frank Müller[b], Frank Mücklich[a]

[a] Chair of Functional Materials, Campus D3 3, Saarland University, 66123 Saarbrücken, Germany
[b] Experimental Physics and Center for Biophysics, Campus E2 9, Saarland University, 66123 Saarbrücken, Germany

ARTICLE INFO

Keywords:
Carbon nanotubes
Electrophoretic deposition
Carbon nanotube coating
Hamaker's law

ABSTRACT

In this study, the coating thickness evolution of pristine and oxidized carbon nanotubes (CNT) on stainless steel substrates is investigated. Potentiostatic electrophoretic deposition (EPD) is used as a coating technique with two different additives, triethylamine (TEA) and magnesium nitrate hexahydrate (Mg-Nit). Moreover, the depositions are conducted at different voltages (50, 100 and 150 V). Confocal laser scanning microscopy is used to determine the thickness of the CNT depositions after 1, 2, 5, 10, 20 and 30 min. Furthermore, the ability of Hamaker's law to accurately predict coating thickness development is investigated for the thickness evolution on stainless steel.

Independent of the additive, the results show that higher voltages lead to increased deposition rates. Comparing the two additives, Mg-Nit generally allows for a higher CNT deposition rate than TEA and forms thicker layers. Coating thickness development can be approximated as linear during the initial 5 min with Mg-Nit and during the initial 20 min with TEA. Finally, Hamaker's law allows for a fairly accurate approximation for the thickness development of CNT coatings with TEA on stainless steel.

1. Introduction

Electrophoretic deposition (EPD) is a technique that enables the deposition of charged particles from a colloidal suspension onto a conductive substrate to obtain homogeneous coatings. After being developed in 1808 by Reuss, EPD was applied for the first time in 1933 to coat platinum cathodes [1]. During EPD, particles dispersed in a suitable solvent move under the influence of an electric field (electrophoresis) towards an oppositely charged electrode immersed in the suspension and deposited on it over time. Primarily, EPD is known as a technique to deposit ceramic particles and has as such been successfully used for a wide range of mostly ceramic particles such as TiO_2 [2], CeO_2 [3], Al_2O_3 [4,5], yttria stabilized zirconia (YSZ) [6], hydroxyapatite [7,8] and bioglass [9] dispersed in various solvents. Considering practical aspects, EPD is a simple and cost-effective, yet efficient coating technique that requires modest equipment and has the ability to form homogeneous coatings even on geometrically complex substrates. At the same time, it is scalable and provides extensive process control by adjusting deposition time, voltage, electrode spacing and suspension composition.

Hamaker developed a linear equation in 1940 aiming to model the deposition process of EPD [10]. With different notations according to Cho et al. [11], Hamaker's equation can be written as follows:

$$w(t) = \int_0^t f \cdot \mu \cdot E \cdot A \cdot C_s \cdot dt \tag{1}$$

with w being the deposition yield in kg, $\mu = \frac{\varepsilon\varepsilon_0\xi}{\eta}$ the electrophoretic mobility in $\frac{m^2}{Vs}$ where ε is the dielectric constant of the solvent, ε_0 the dielectric constant of the vacuum in $\frac{As}{Vm}$, ξ the zeta potential in V and η the viscosity in $Pa \cdot s$, E the electric field strength in $\frac{V}{m}$, A the coated area in m^2, C_s the particle concentration in $\frac{kg}{m^3}$ and f an efficiency factor (also referred to as "sticking parameter"), depending on whether each particle reaching the anode will contribute to the layer. Assuming the simplification that all factors are time-independent, the integral transforms to a multiplication:

$$w(t) = f \cdot \mu \cdot E \cdot A \cdot C_s \cdot t \tag{2}$$

Ever since Thomas et al. deposited multiwall carbon nanotubes (CNTs) onto a metallic surface [12], EPD has started to generate wider interest for being applicable to sp^2-hybridized carbon nanoparticles, as it has proven to be an effective technique to form homogeneous carbon nanoparticle coatings. This applies particularly to CNT coatings for tribological applications [13–15], wettability tuning [14], in superca-

* Corresponding author.
E-mail address: timothy.maclucas@uni-saarland.de (T. MacLucas).

https://doi.org/10.1016/j.cartre.2023.100265
Received 31 March 2023; Received in revised form 2 May 2023; Accepted 2 May 2023

pacitors [16] or vertically aligned CNTs on carbon fiber [17]. Moreover, EPD has proven to successfully deposit carbon onions [18,19], carbon nanohorns [20], but also graphene quantum dots [21] and other graphene-related materials [22].

In order to obtain coatings with EPD, the dispersed particles must have a surface charge in suspension. Carbon nanoparticles with sp^2 hybridization generally show a negative surface charge stemming from the deprotonation of oxygen-containing functional groups such as hydroxy or carboxy groups [23]. These groups are incorporated during synthesis, primarily at the caps but also on the side walls [24]. This is facilitated by their curved structure and the associated increased reactivity due to pyramidalization of the π-orbitals [25]. However, further oxidizing CNTs in a strongly acidic environment enhances the incorporation of functional groups and, thus, the negative surface charge which will influence the deposition kinetics. Functionalization may be advantageous as shown by Gojny and Schulte, where functionalizing CNTs lead to improved interfacial adhesion of CNTs in epoxy composites [26].

Deposition results during EPD can be improved by using additives, of which there is a wide variety, such as salts like nickel chloride [27] or quaternary ammonium salts [28] and nitrates, most prominently aluminium nitrate [29] and magnesium nitrate hexahydrate (Mg-Nit) [30,31]. The latter, along with triethylamine (TEA) [13,14], are amongst the most commonly used additives for CNT deposition. When using Mg-Nit, Mg^{2+} ions non-covalently attach to the negative surface groups causing the deposition to occur on the cathode. The use of TEA on the other hand leads to an anodic deposition [32].

In this work, the layer thickness evolution of CNT coatings on stainless steel substrates is studied during potentiostatic EPD with TEA and Mg-Nit as additives. Secondly, a linear approximation of CNT layer growth based on Hamaker's law was performed in order to precisely predict coating thickness, which can save a significant amount of characterization time and, therefore, increases applicability.

2. Materials and methods

2.1. Materials

Multiwall CNT acquired from Graphene Supermarket (Calverton, USA) were used in this study. According to the provider, the outer diameter varies between 30 and 85 nm, with a length of 10-15 µm and a carbon fraction above 94 %. Triethylamine (99.0 %, Chemsolute, Germany) and magnesium nitrate hexahydrate (Merck, Germany) were used as additives. As substrates, platelets (20×20×1 mm^3) of AISI 304 austenitic stainless steel (BRIO Kontrollspiegel GmbH, Germany) with mirror polished (S_q = 9 nm) surface were utilized.

2.2. Functionalization and dispersion preparation

Prior to the deposition, a batch of CNTs were functionalized with a HNO_3/H_2SO_4 mixture (v/v ratio 3:1). In a first step, the CNTs were dispersed in the acid mixture via ultrasonication (Bandelin, Sonorex Super RK 514 Bh, 35 kHz-860 W) for 10 min. Next, the CNTs were oxidized in the mixture for 72 h at 80°C under reflux. Subsequently, the CNTs were filtered and washed with deionized water until the pH of the permeated water reached 7. Finally, the functionalized CNTs were dried in an oven overnight at 100°C.

Each dispersion consists of 80 ml of isopropanol (IPA) and 8 mg (corresponds to a concentration of 0.1 mg/ml) of either pristine (p-CNTs) or oxidized CNTs (o-CNTs). In addition, either 10 ml of TEA or 2 mg of Mg-Nit were used as additives to support the deposition process. The four following suspensions were used:

- IPA + TEA + p-CNT
- IPA + TEA + o-CNT
- IPA + Mg-Nit + p-CNT
- IPA + Mg-Nit + o-CNT

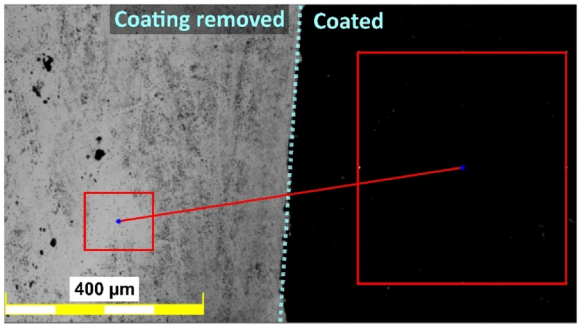

Fig. 1. Top view confocal laser scanning micrograph of a frontier between a CNT-coated part of the sample surface (right) and another part where the coating was removed (left). The coating thickness was determined by measuring the height difference between these two regions of interest using CLSM.

The CNTs were dispersed with an Ultra-Turrax (T25 digital, IKA, Germany) shear mixer for 5 min at 5000 rpm followed by 10 min of ultrasonication in the same device mentioned above.

2.3. Electrophoretic deposition

Two stainless steel platelets serving as electrodes were immersed in the dispersion and connected to a DC power supply (Consort EV3020, Carl Roth, Germany). Deposition was conducted in potentiostatic mode at three different voltages (50 V, 100 V and 150 V) for the following deposition times: 1, 2, 5, 10, 20 and 30 min. For each set of parameters one sample was coated.

2.4. Characterization

To assess the degree of functionalization, X-Ray Photoelectron Spectroscopy (XPS) was used to determine the oxygen content. XPS measurements were performed with an ESCA MkII spectrometer (Vacuum Generators) in normal emission mode using Al-Kα excitation ($\hbar\bullet\omega$ = 1486.6 eV) and a 150°-type hemispherical analyzer. Survey spectra were recorded with a pass energy of 50 eV, detail spectra (for analysis of elemental composition) were recorded with a pass energy of 20 eV. The calibration was made to the Au-4f $_{7/2}$ line at 83.80 eV.

Zeta potential measurements were performed with a Malvern Panalytical Zetasizer at a temperature of 20°C with a refractive index of 2.47 and an absorption of 0.99.

A Haake Rotational Rheometer (RheoStress 1, Thermo Fisher Scientific) was used to determine the viscosity of the EPD dispersions. Steady shear measurements were conducted at room temperature in constant-stress mode. The ratio of cup to bob radii was 1.0847 with a gap of 1.45 mm.

To determine the thickness of the CNT coatings, an Olympus LEXT OLS4100 confocal laser scanning microscope (CLSM) with a 50x objective (NA: 0.95) at a laser wavelength of 405 nm was used. As illustrated in Fig. 1, coating thickness was measured by comparing two regions of interest and forming the difference. To verify the CLSM data, coating thicknesses were also measured using scanning electron micrographs that were prepared using a Helios NanoLab 600 dual beam workstation (SEM/FIB, by Field Electron and Ion Company) at an acceleration voltage of 5 kV and a current of 1.4 nA.

3. Results and discussion

3.1. Dispersion, CNT and coating characterization

Fig. 2 shows the XPS survey spectra of p- and o-CNTs. The spectra display mainly the C1s and O1s peaks as well as the C-KVV and

Table 1
Overview of the characterization data. Carbon and oxygen content of p- and o-CNTs measured by XPS. Zeta potential of the CNTs in different dispersions with and without additives. Viscosity for the dispersions and for IPA.

	Pristine			Oxidized		
Carbon (at. %)	98.62			96.40		
Oxygen (at. %)	1.38			3.60		
Additive	-	TEA	Mg-Nit	-	TEA	Mg-Nit
Zeta potential (mV)	− 15.27 ± 1.50	− 10.99 ± 1.16	− 6.34 ± 0.98	− 29.63 ± 1.89	− 20.73 ± 1.31	+ 14.30 ± 0.86
Viscosity (mPa•s)	-	1.89 ± 0.08	2.37 ± 0.09	-	1.95 ± 0.08	2.24 ± 0.07

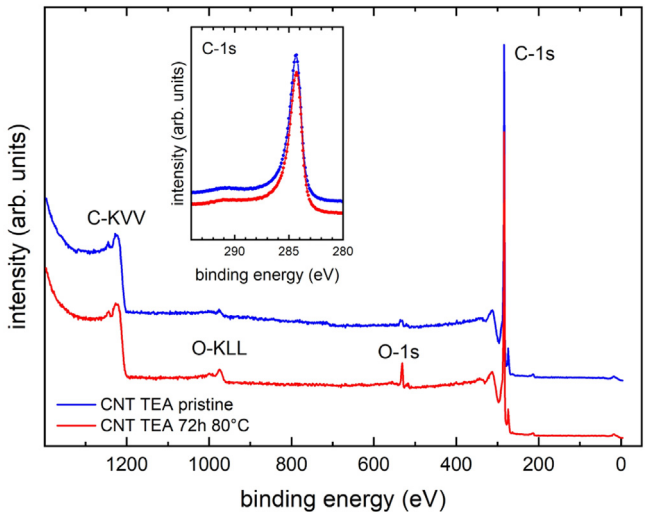

Fig. 2. XPS survey spectra of p- (blue) and o-CNTs (red). Inset: C1s detail spectra.

O-KKL Auger peaks with no traces of other elements. The C1s detail spectra (inset) of both samples display a narrow main contribution at 284.3 eV (as characteristic for sp^2 C bonds) and the small broad shake-up π satellite around 290.5 eV [33]. Between the main peak and the π satellite only small contributions from C-O, C-OH and/or C=O species contribute to a small shoulder of the main peak. The analysis of the C1s and O1s spectra (peak intensity above Shirley background [34] scaled with the photoemission cross sections by Yeh and Lindau [35]) provides atomic ratios of C:O = 98.62:1.38 and 96.40:3.60 for p- and o-CNTs, respectively (see Tab. 1) showing that the acid-functionalization leads to a considerable increase of the CNTs' oxygen content. The additional oxygen is incorporated to a large degree in the form of oxygen-containing functional surface groups such as carbonyl and hydroxy groups [23,36], but mainly carboxy groups [37].

To determine the CNTs' surface charge in solution, the zeta potential was measured while the particles are dispersed in different suspensions (results shown in Table 1). Comparing p- and o-CNTs reveals that the acid-functionalization causes the zeta potential in pure IPA to become more negative, roughly by a factor of 2.5. This outcome was to be expected due to the further incorporation of carbonyl, hydroxy or carboxy groups. Carboxy groups in particular are known to deprotonate in solution, and form carboxylate anions which dominate the interaction with the additives and provide the CNTs with negative surface charges [37].

Adding TEA to the deposition suspension seems to attenuate the CNTs negative zeta potential (regardless of oxidation state). We believe that, to a certain degree, TEA protonates to ammonium (NH_4^+) and subsequently non-covalently complexes some of the carboxylates on the surface of the CNTs, thereby mitigating the negative charge. The presence of Mg-Nit has the same yet more enhanced effect. In solution, Mg-Nit dissolves into Mg^{2+} and NO_3^-. The former also forms complexes with the surface groups. In the case of o-CNT, the zeta potential completely shifts to become positive.

The viscosities of the different dispersions were determined to model the coating thickness development according to Hamaker's equation. In general, low-viscosity suspensions are preferred as they pose less resistance to particle motion during EPD. The data presented in Table 1 indicate that CNT/Mg-Nit dispersions exhibit an increased dispersion viscosity compared to CNT/TEA dispersions. This can be explained by higher electrostatic forces from bivalent Mg^{+2} ions leading to stronger attracting forces between the CNTs which generally increases the viscosity. In addition to that, the viscosity of pure TEA is low (0.347 mPa•s [38]) resulting in an overall viscosity decrease of the CNT/TEA dispersion.

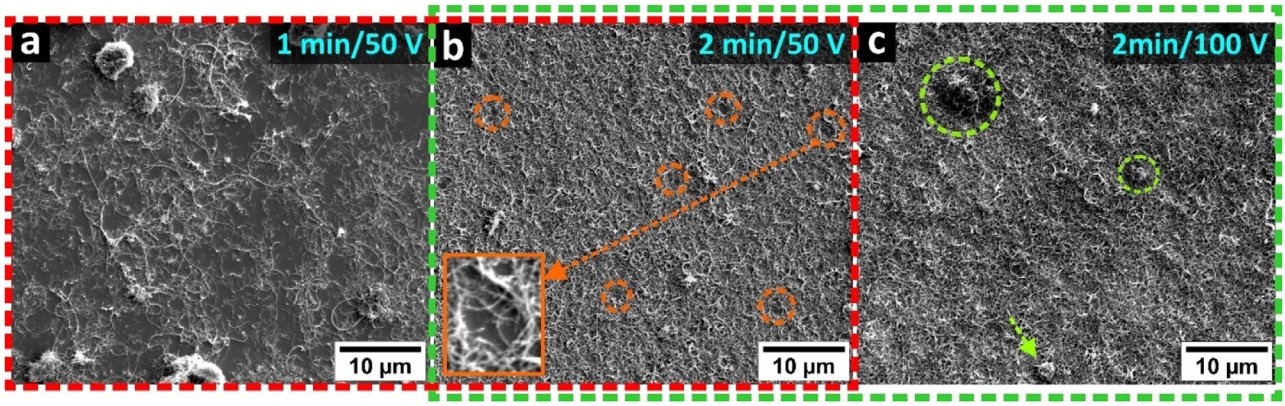

Fig. 3. Top view scanning electron micrographs showing the coating thickness development of o-CNTs deposited with TEA (a) after 1 min at 50 V, (b) 2 min at 50 V and (c) 2 min at 100 V.

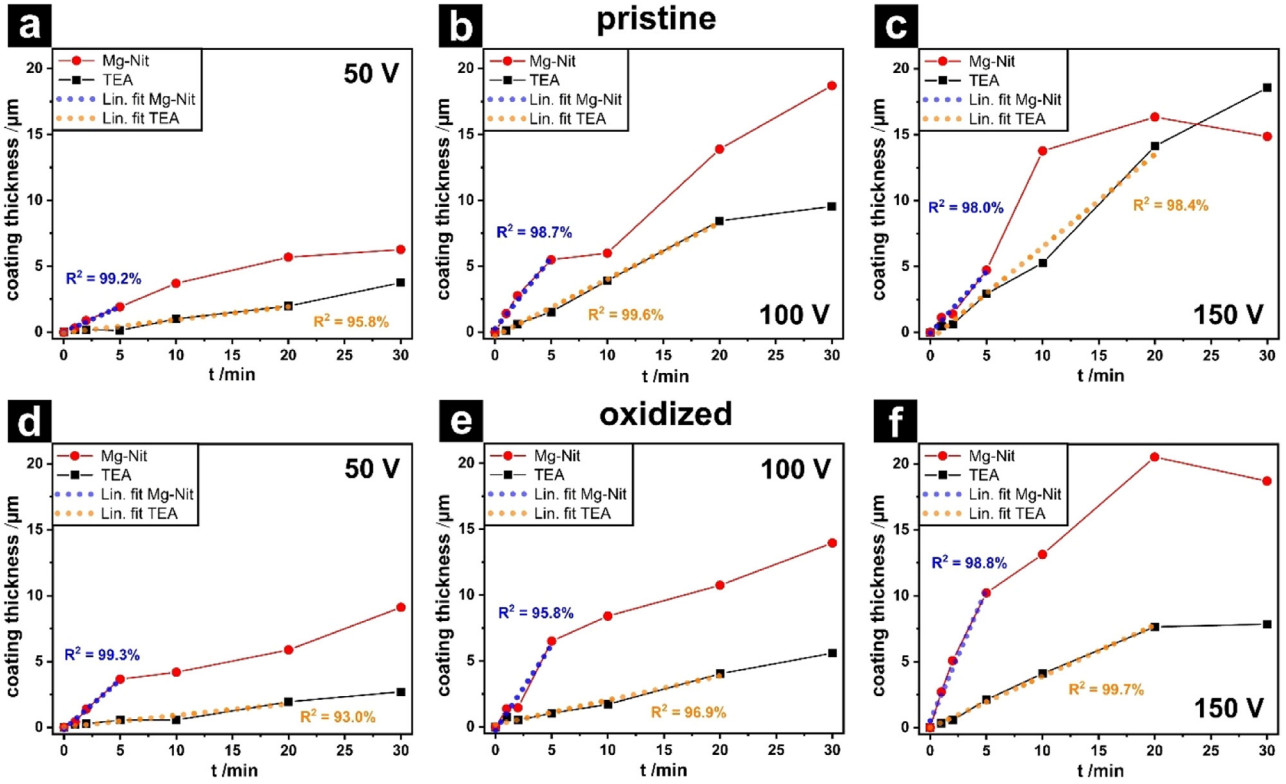

Fig. 4. Coating thickness development (measured using CLSM) in the presence of TEA and Mg-Nit for pristine (a-c) and oxidized (d-f) CNTs at 50, 100 and 150 V.

In Fig. 3, top view scanning electron micrographs at different stages of the thickness development of o-CNTs deposited with TEA are shown. The first deposition after 1 min at 50 V shows individual o-CNTs (randomly oriented) together with a few o-CNT agglomerates as well as the underlying substrate (Fig. 3a). When the deposition time is doubled (Fig. 3b), the coating covers the substrate almost completely, however, the underlying substrate is still recognizable in some locations (orange markings). Fig. 3c shows, that doubling the voltage over a deposition period of 2 min results in a coating that fully covers the surface and incorporates large agglomerates (green markings).

3.2. Development of CNT coating thickness

Fig. 4 shows the temporal coating thickness development of pristine (Fig. 4a-c) and oxidized (Fig. 4d-f) CNTs deposited with either TEA or Mg-Nit as an additive at 50 V, 100 V and 150 V measured by CLSM. The CNT coatings generally grow thicker as deposition time increases, regardless of the oxidation state or the additive. Moreover, higher voltages typically lead to higher deposition rates which is consistent with the literature [39,40]. Initially, the thickness development can be approximated as linear. In the presence of Mg-Nit, this applies during the first 5 min ($95.8\% < R^2 < 99.3\%$). Afterwards, the curve kinks downwards in most cases. This agrees well with the findings of Gardeshzadeh and Rasouli who investigated the deposition yield of multiwall CNTs dispersed in ethanol with Mg-Nit as an additive [40]. TEA exhibits similar behaviour, however, linear growth is maintained for roughly 20 min ($93.0\% < R^2 < 99.7\%$).

The difference in coating thickness between TEA and Mg-Nit tends to be more pronounced at higher voltages and longer deposition periods. However, p- and o-CNTs deposited in the presence of Mg-Nit at 150 V demonstrate that longer deposition periods and higher deposition rates do not necessarily result in thicker coatings. In those cases, the deposition rate starts to decline, and it appears as if a maximum is reached around 20 min (Fig. 4c and f). This maximum represents a saturation state where the CNT deposition shields and, thus, neutralizes the electrical field of the underlying electrode. This is in agreement with results obtained by Singh et al. for graphene oxide-polymer composite at 10 V [41].

Consequently, layer thickness decreases as both individual CNTs and CNT agglomerations detach from the deposition due to the lack of an attractive force. Decreasing CNT concentration in the suspension over the course of the deposition is another factor contributing to the slowdown of the deposition rate [40]. Saturation seems to occur in TEA also, as demonstrated by the o-CNTs' flattening deposition rate after 20 min at 150 V (Fig. 4f) or possibly exceeded it already. Achieving saturation below 150 V seems to require deposition periods beyond 30 min.

Within a study published in 2004, Wang and co-workers used EPD to coat copper substrate with ZnO nanoparticles [42]. The development of layer thickness was studied over time at deposition voltages of 20, 60 and 100 V. Initially, the ZnO layer grew almost linearly. After a certain period of time, the line starts to flatten and eventually plateau. Overall, these results correspond well with ours.

With just over 20 µm, o-CNTs with Mg-Nit at 150 V produce the thickest coatings. Several factors contribute to this. First, the highest voltage results in the strongest electrical field and hence the highest deposition rate prior to saturation. Secondly, functionalization increases the amount of superficial carboxyl groups and, thus, leads to an enhancement of the negative surface charge [23,43], as corroborated by the respective zeta potentials listed in Table 1. Moreover, Yi and Chen proved that Ca^{2+} forms bidentate rather than monodentate complexes with carboxyl groups on the surface of multiwalled CNTs [37]. Ca^{2+} binds more effectively to the carboxyl groups on highly

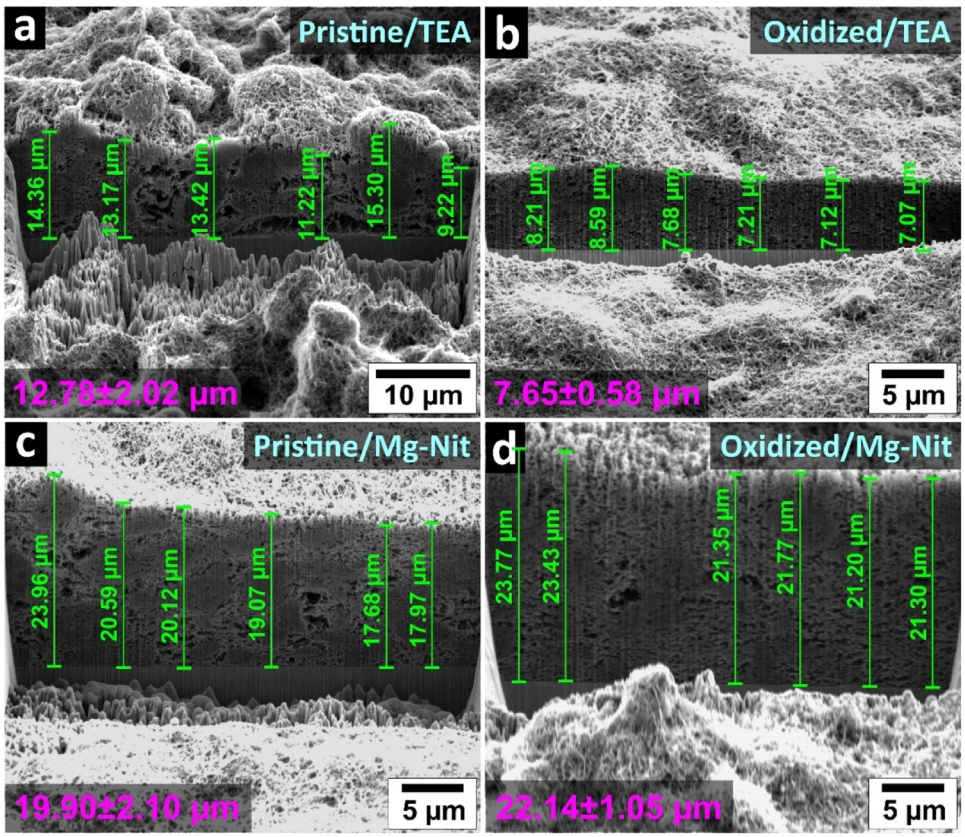

Fig. 5. FIB cross-sections of the CNT coatings (without protective coating) after a deposition time of 20 min at 150 V with (a) pristine CNTs with TEA, (b) oxidized CNTs with TEA, (c) pristine CNTs with Mg-Nit and (d) oxidized CNTs with Mg-Nit.

oxidized CNTs compared to lower oxidized CNTs because there is a greater probability that a larger proportion of carboxyl groups will be in sufficient proximity to form bidentate complexes on highly oxidized CNT surfaces. In isopropanol, Mg-Nit dissolves to nitrate and Mg^{2+}, which behaves similarly to Ca^{2+} (both bivalent). Once again, this is supported by the zeta potentials (Table 1) which shows that the addition of Mg-Nit leads to a positive charge on o-CNTs opposed to the p-CNTs.

Focused ion beam (FIB) was used to prepare cross-sections of the CNT coatings and their thickness was measured using SEM to validate the CLSM measurements. Contrary to the standard FIB procedure, protective Pt coatings were omitted due to the CNTs mechanical flexibility which otherwise resulted in the compression of the coatings. Fig. 5 shows electron micrographs with coating thicknesses of pristine and oxidized CNTs deposited with TEA and Mg-Nit after 20 min at 150 V, which are in good agreement with coating thicknesses measured by CLSM (additional FIB cross-sections after a deposition time of 10 min at 50 V are shown in S1 in the Supplementary Information). As previously mentioned, the increase in coating thickness can be approximated as linear during the initial 20 min of deposition using TEA and during the initial 5 min using Mg-Nit as an additive. Fig. 6 shows the linear regression lines fitted to the coating thicknesses deposited at 50 V, 100 V and 150 V obtained by CLSM. The corresponding Hamaker lines, which were calculated using experimentally determined parameters (Tables 1 and 2), are plotted alongside. To assess whether Hamaker is suitable for accurately predicting coating thickness evolution, we introduce a slope ratio $\beta = \frac{slope\ (linear\ fit)}{slope\ (Hamaker\ fit)}$ ($\beta = 1$ represents perfect conformity).

Independent of oxidation or deposition voltage, β_{TEA} is relatively close to 1, hence Hamaker's equation can be used for a rough approximation of the coating thickness when the CNT suspension contains TEA as an additive. This is not the case for Mg-Nit suspensions since $\beta_{Mg\text{-}Nit}$ deviates strongly from 1, meaning that the actual deposition rate is considerably higher than predicted by Hamaker's equation.

Table 2
Overview of the parameters used for Hamaker modelling.

A	$2.64 \cdot 10^{-4}$ m^2
E	3333.33 V·m^{-1} (50 V)
(assuming an electrode distance	6666.66 V·m^{-1} (100 V)
of 1.5 cm)	10000.00 V·m^{-1} (150 V)
C_S	0.10 kg·m^{-3}
ε (IPA)	20.18 [44]
ε_0	$8.85 \cdot 10^{-12}$ A·s·V^{-1}·m^{-1}

Analyzing each of the parameters considered by Hamaker, it is reasonable to state that the vast majority of them remain constant throughout the deposition. Particularly, considering that there are no significant changes in Zeta potential and viscosity, therefore, the electrophoretic mobility will remain constant. The same is true for the applied electric field (interelectrode distance is constant) and deposition area. Thus, the only two parameters in Hamaker's equation that indeed change with time are the efficiency factor f and the concentration. Considering that the concentration is expected to diminish with time, the only compensating parameter left is f. The increase in yield can thus be traced back to a high compactness of the CNTs deposited with Mg-Nit (as observable in Fig. 5c and d), likely associated to a stronger interaction of the bivalent ions with the applied electric field.

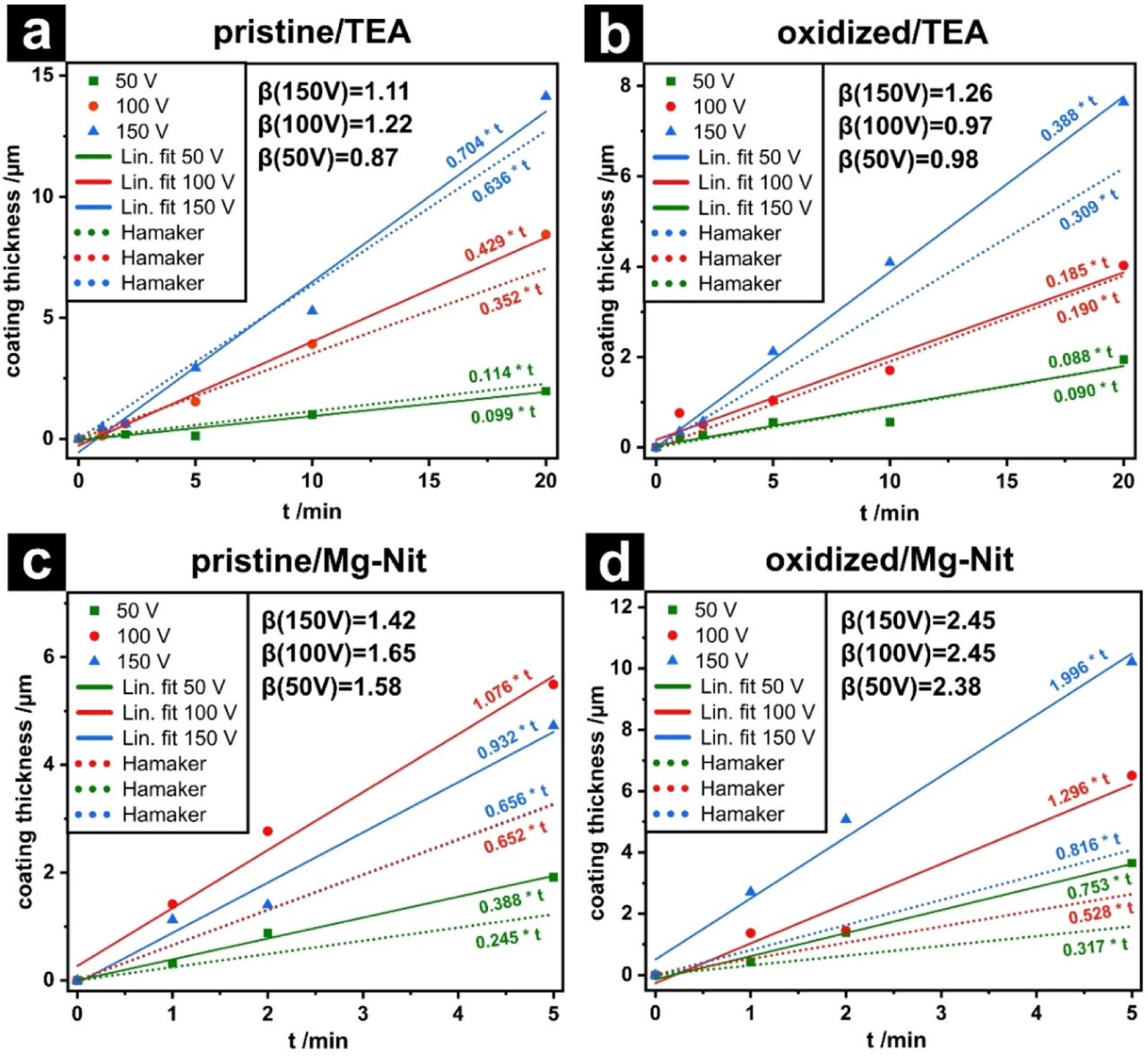

Fig. 6. Linear coating thickness development with TEA during the initial 20 min of deposition for (a) pristine and (b) oxidized CNT. Linear coating thickness development with Mg-Nit during the initial 5 min of deposition for (c) pristine and (d) oxidized CNT. The dotted lines represent the corresponding Hamaker lines.

4. Conclusion

Within this study, the temopral coating thickness development of pristine and oxidized CNTs on stainless steel substrates were investigated. EPD was used as a coating technique with dispersions containing two different additives over a range of voltages. The following are the key findings of this work:

- Regardless of additive or oxidation state, the coating thickness grows linearly during the initial phase of the deposition. The duration of that period depends on the additive.
- After deposition times of 20 min and more, coating growth indicates saturation. This becomes particularly evident at higher voltages.
- Regarding the additives, Mg-Nit typically exhibits higher deposition rates and, thus, forms thicker coatings than TEA over the same deposition period.
- Hamaker's equation can serve as a rough estimation for the thickness of CNT coatings deposited from dispersions containing TEA.

Declaration of Competing Interest

The authors declare that they have no known competing financial interests or personal relationships that could have appeared to influence the work reported in this paper.

Data availability

Data will be made available on request.

Acknowledgements

The activities within this work were financially supported by the State of Saarland from the European Regional Development Fund (Europäischer Fond für Regionale Entwicklung, EFRE) and Deutsche Forschungsgemeinschaft (DFG, German Research Foundation) within the project MU 959/47-1. Further, we acknowledge support by Saarland University within the 'Open Access Publication Funding' program.

Frank Müller acknowledges partial support from the German Research Foundation (DFG) via the Collaborative Research Center SFB 1027. Furthermore, the authors wish to thank Daniela Foetz, formerly part of the research group for structural and functional ceramics at Saarland University for granting the authors access to the viscosimeter as well as Rebekka Christmann, formerly part of the drug delivery department of the Helmholtz Institute for Pharmaceutical Research Saarland, for her assistance with the zeta potential measurements.

Supplementary materials

Supplementary material associated with this article can be found, in the online version, at doi:10.1016/j.cartre.2023.100265.

References

[1] E. Harsanyi, Method of coating radiant bodies, 1933.
[2] S. Yanagida, A. Nakajima, Y. Kameshima, N. Yoshida, T. Watanabe, K. Okada, Preparation of a crack-free rough titania coating on stainless steel mesh by electrophoretic deposition, Mater. Res. Bull. 40 (2005) 1335–1344.
[3] I. Zhitomirsky, A. Petric, Electrolytic and electrophoretic deposition of CeO2 films, Mater. Lett. 40 (1999) 263–268.
[4] B. Ferrari, R. Moreno, Electrophoretic deposition of aqueous alumina slips, J. Eur. Ceram. Soc. 17 (1997) 549–556.
[5] B. Ferrari, R. Moreno, The conductivity of aqueous Al2O3 slips for electrophoretic deposition, Mater. Lett. 28 (1996) 353–355.
[6] T. Ishihara, K. Sato, Y. Takita, Electrophoretic Deposition of Y2O3-Stabilized ZrO2 Electrolyte Films in Solid Oxide Fuel Cells, J. Am. Ceram. Soc. 79 (1996) 913–919.
[7] P. Ducheyne, S. Radin, M. Heughebaert, J.C. Heughebaert, Calcium phosphate ceramic coatings on porous titanium: effect of structure and composition on electrophoretic deposition, vacuum sintering and in vitro dissolution, Biomaterials 11 (1990) 244–254.
[8] T.M. Sridhar, U.K. Mudali, M. Subbaiyan, Preparation and characterisation of electrophoretically deposited hydroxyapatite coatings on type 316L stainless steel, Corros. Sci. 45 (2003) 237–252.
[9] A.R. Boccaccini, E.J. Minay, D. Krause, Bioglass® coatings on superelastic NiTi wires by electrophoretic deposition (EPD), Key Eng. Mater. Trans. Tech. Publ. (2006) 219–224.
[10] H.C. Hamaker, Formation of a deposit by electrophoresis, Trans. Faraday Soc. 35 (1940) 279–287.
[11] J. Cho, K. Konopka, K. Rozniatowski, E. García-Lecina, M.S.P. Shaffer, A.R. Boccaccini, Characterisation of carbon nanotube films deposited by electrophoretic deposition, Carbon 47 (2009) 58–67.
[12] B.J.C. Thomas, M.S.P. Shaffer, S. Freeman, M. Koopman, K.K. Chawla, A.R. Boccaccini, Electrophoretic Deposition of Carbon Nanotubes on Metallic Surfaces, Key Eng. Mater. 314 (2006) 141–146.
[13] L. Reinert, F. Lasserre, C. Gachot, P. Grützmacher, T. MacLucas, N. Souza, F. Mücklich, S. Suarez, Long-lasting solid lubrication by CNT-coated patterned surfaces, Sci. Rep. 7 (2017) 42873.
[14] T. Maclucas, S. Schütz, S. Suarez, F. Mücklich, Surface protection of austenitic steels by carbon nanotube coatings, Surf. Topogr. Metrol. Prop. 6 (2018) 14005.
[15] C. Schäfer, L. Reinert, T. MacLucas, P. Grützmacher, R. Merz, F. Mücklich, S. Suarez, Influence of Surface Design on the Solid Lubricity of Carbon Nanotubes-Coated Steel Surfaces, Tribol. Lett. 66 (2018) 89.
[16] C. Du, N. Pan, Supercapacitors using carbon nanotubes films by electrophoretic deposition, J. Power Sources. 160 (2006) 1487–1494.
[17] L. Li, W. Liu, F. Yang, W. Jiao, L. Hao, R. Wang, Interfacial reinforcement of hybrid composite by electrophoretic deposition for vertically aligned carbon nanotubes on carbon fiber, Compos. Sci. Technol. 187 (2020) 107946.
[18] C. Zhu, T. Liu, F. Qian, W. Chen, S. Chandrasekaran, B. Yao, Y. Song, E.B. Duoss, J.D. Kuntz, C.M. Spadaccini, M.A. Worsley, Y. Li, 3D printed functional nanomaterials for electrochemical energy storage, Nano Today 15 (2017) 107–120.
[19] P. Huang, D. Pech, R. Lin, J.K. McDonough, M. Brunet, P.L. Taberna, Y. Gogotsi, P. Simon, On-chip micro-supercapacitors for operation in a wide temperature range, Electrochem. Commun. 36 (2013) 53–56.
[20] T. MacLucas, S. Suarez, On the solid lubricity of electrophoretically deposited carbon nanohorn coatings, Lubricants 7 (2019) 62.
[21] T.D. Nguyen, O. Geuli, L.P. Yeo, S. Magdassi, D. Mandler, A.I.Y. Tok, Additive-free electrophoretic deposition of graphene quantum dots thin films, Chem. Eur. J. 25 (2019) 16573–16581.
[22] M. Diba, D.W.H. Fam, A.R. Boccaccini, M.S.P. Shaffer, Electrophoretic deposition of graphene-related materials: A review of the fundamentals, Prog. Mater. Sci. 82 (2016) 83–117.
[23] V. Datsyuk, M. Kalyva, K. Papagelis, J. Parthenios, D. Tasis, A. Siokou, I. Kallitsis, C. Galiotis, Chemical oxidation of multiwalled carbon nanotubes, Carbon 46 (2008) 833–840.
[24] S. Niyogi, M.A. Hamon, H. Hu, B. Zhao, P. Bhowmik, R. Sen, M.E. Itkis, R.C. Haddon, Chemistry of single-walled carbon nanotubes, Acc. Chem. Res. 35 (2002) 1105–1113.
[25] R.C. Haddon, Chemistry of the fullerenes: The manifestation of strain in a class of continuous aromatic molecules, Science 261 (1993) 1545–1550.
[26] F.H. Gojny, K. Schulte, Functionalisation effect on the thermo-mechanical behaviour of multi-wall carbon nanotube/epoxy-composites, Compos. Sci. Technol. 64 (2004) 2303–2308.
[27] D.A. Kurnosov, A.S. Baturin, A.S. Bugaev, K.N. Nikolski, R.G. Tchesov, E.P. Sheshin, Influence of the interelectrode distance in electrophoretic cold cathode fabrication on the emission uniformity, Appl. Surf. Sci. 215 (2003) 232–236.
[28] P.V. Kamat, K.G. Thomas, S. Barazzouk, G. Girishkumar, K. Vinodgopal, D. Meisel, Self-assembled linear bundles of single wall carbon nanotubes and their alignment and deposition as a film in a dc field, J. Am. Chem. Soc. 126 (2004) 10757–10762.
[29] G. Zhu, L. Pan, T. Lu, X. Liu, T. Lv, T. Xu, Z. Sun, Electrophoretic deposition of carbon nanotubes films as counter electrodes of dye-sensitized solar cells, Electrochim. Acta. 56 (2011) 10288–10291.
[30] K. Yu, Z. Zhu, Q. Li, W. Lu, Electronic properties and field emission of carbon nanotube films treated by hydrogen plasma, Appl. Phys. A Mater. Sci. Process. 77 (2003) 811–817.
[31] S. Santhanagopalan, F. Teng, D.D. Meng, High-Voltage Electrophoretic Deposition for Vertically Aligned Forests of One-Dimensional, Nanoparticles 27 (2011) 561–569.
[32] M.F. De Riccardis, D. Carbone, A. Rizzo, A novel method for preparing and characterizing alcoholic EPD suspensions, J. Colloid Interface Sci. 307 (2007) 109–115.
[33] X. Chen, X. Wang, D. Fang, A review on C1s XPS-spectra for some kinds of carbon materials, Fullerenes, Nanotub. Carbon Nanostruct. 28 (2020) 1048–1058.
[34] D.A. Shirley, High-resolution X-ray photoemission spectrum of the valence bands of gold, Phys. Rev. B. 5 (1972) 4709.
[35] J.J. Yeh, I. Lindau, Atomic subshell photoionization cross sections and asymmetry parameters: 1≤ Z≤ 103, At. Data Nucl. Data Tables 32 (1985) 1–155.
[36] I. Mazov, V.L. Kuznetsov, I.A. Simonova, A.I. Stadnichenko, A.V Ishchenko, A.I. Romanenko, E.N. Tkachev, O.B. Anikeeva, Oxidation behavior of multiwall carbon nanotubes with different diameters and morphology, Appl. Surf. Sci. 258 (2012) 6272–6280.
[37] P. Yi, K.L. Chen, Influence of Surface Oxidation on the Aggregation and Deposition Kinetics of Multiwalled Carbon Nanotubes in Monovalent and Divalent Electrolytes, Langmuir 27 (2011) 3588–3599.
[38] D.R. Lide, CRC Handbook of Chemistry and Physics, CRC Press, Boca Raton, 2010.
[39] I. Zhitomirsky, L. Gal-Or, Electrophoretic deposition of hydroxyapatite, J. Mater. Sci. Mater. Med. 8 (1997) 213–219.
[40] A.R. Gardeshzadeh, S. Rasouli, Kinetic investigation of carbon nanotube deposition by DC electrophoretic technique, (2011).
[41] B.P. Singh, B.K. Jena, S. Bhattacharjee, L. Besra, Development of oxidation and corrosion resistance hydrophobic graphene oxide-polymer composite coating on copper, Surf. Coatings Technol. 232 (2013) 475–481.
[42] Y.C. Wang, I.C. Leu, M.H. Hon, Kinetics of electrophoretic deposition for nanocrystalline zinc oxide coatings, J. Am. Ceram. Soc. 87 (2004) 84–88.
[43] K.A. Wepasnick, B.A. Smith, K.E. Schrote, H.K. Wilson, S.R. Diegelmann, D.H. Fairbrother, Surface and structural characterization of multi-walled carbon nanotubes following different oxidative treatments, Carbon 49 (2011) 24–36.
[44] M.T. Khimenko, V.V Litinskaya, G.P. Khomenko, Vliyanie kontsentratsii na polyarizuemost'molekuly izopropilovogo spirta v dimetilsul'fokside [Effect of concentration on the molecule polarizability of isopropyl alcohol in dimethyl sulphoxide], Zh. Fiz. Khim. 56 (1982) 867–870.